10 March 2025

Diamondiyne: A 3D carbon allotrope with mixed valence hybridization

Yizhou Yang[2], Jie Xu[1], Yanyan Chen[3], Yu Xia[4], Clara Schäfer[1], Martin Ratsch[1], Martin Rahm[5], Tom Willhammar[4], Karl Börjesson[1]

1. University of Gothenburg
2. Chalmers
3. Carpona AB
4. Stockholm University
5. Chalmers University of Technology

Abstract

Carbon is arguably the most versatile element in the periodic table. It can form bonds to other elements in one-, two- and three-dimensions, allowing the formation of structurally and electronically diverse materials. Carbon allotropes, materials made only of carbon, were for long limited to diamond, graphite, fullerene, carbon nanotubes, and graphene. However, recently a series of zero- one- and two-dimensional carbon allotropes have been made. Until now, diamond is the only known three-dimensional carbon allotrope. Here we report the successful synthesis of a new 3D carbon allotrope, which we refer to as diamondiyne. The synthesis of diamondiyne is performed using inexpensive laboratory glassware. It is formed as a film at a liquid-liquid interface, and we show that the method is scalable in both the thickness and lateral area of the film. The received films are polycrystalline, and the crystal structure has been confirmed using transmission electron microscopy. Our results enrich the carbon allotrope family, enabling non-naturally occurring ones extending in full 3D space. New carbon allotropes have historically found widespread use in materials science, and we look forward to what applications might emerge for diamondiyne.

Keywords

covalent organic framework, allotrope, carbon allotrope, COF

Diamondiyne: A 3D carbon allotrope with mixed valence hybridization

Yizhou Yang[1,2], Jie Xu[1], Yanyan Chen[3], Yu Xia[4], Clara Schäfer[1,5], Martin Ratsch[1], Martin Rahm[2], Tom Willhammar[4] and Karl Börjesson[1]*

[1]Department of Chemistry and Molecular Biology, University of Gothenburg, Medicinaregatan 7B, 413 90 Gothenburg, Sweden

[2]Department of Chemistry and Chemical Engineering, Chalmers University of Technology, Kemigården 4, 412 58 Gothenburg, Sweden

[3]Carpona AB, Erik Dahlbergsgatan 11A, 411 26, Göteborg, Sweden

[4]Department of Chemistry, Stockholm University, 106 91 Stockholm, Sweden

[5]Present address: Nano-Science Center & Department of Chemistry, University of Copenhagen, Universitetsparken 5, 2100 Copenhagen, Denmark

Carbon is arguably the most versatile element in the periodic table. It can form bonds to other elements in one-, two- and three-dimensions, allowing the formation of structurally and electronically diverse materials[1]. Carbon allotropes, materials made only of carbon, were for long limited to diamond, graphite, fullerene, carbon nanotubes, and graphene[2]. However, recently a series of zero-[3-5] one-[6-8] and two-dimensional[9-14] carbon allotropes have been made. Until now, diamond is the only known three-dimensional carbon allotrope. Here

we report the successful synthesis of a new 3D carbon allotrope, which we refer to as diamondiyne. The synthesis of diamondiyne is performed using inexpensive laboratory glassware. It is formed as a film at a liquid-liquid interface, and we show that the method is scalable in both the thickness and lateral area of the film. The received films are polycrystalline, and the crystal structure has been confirmed using transmission electron microscopy. Our results enrich the carbon allotrope family, enabling non-naturally occurring ones extending in full 3D space. New carbon allotropes have historically found widespread use in materials science, and we look forward to what applications might emerge for diamondiyne.

The first documented trial of making diamondiyne was made by Feldman about 30 years ago[15], around the same time as fullerenes and carbon nanotubes were discovered. One important advance at the time was the synthesis of tetraethynylmethane, the basic building block needed for the synthesis of diamondiyne[16,17]. Following the discovery of graphene in 2005, interest in finding more carbon allotropes surged, resulting in a steep increase in the number of theoretically predicted structures, which currently stands at 1635[18]. The synthetic effort has just started to see a similar increase, with the synthesis of several new zero-[3-5], one-[7,8], and two-dimensional[10-14] allotropes being reported. Among these, is a structure that can be viewed as an expanded version of graphene, in which benzene rings are connected at every vertex by alkyne triple bonds[13,14]. The latter structure is composed of carbon atoms with different kinds of valance hybridization (sp^2 and sp), making it particularly relevant for comparison against the material presented herein.

By allowing for mixtures of valence hybridizations of carbon, more diverse structures become possible. For example, by introducing sp hybridized carbons in the diamond structure, a new family of theoretical 3D carbon allotropes, referred to as diamondynes[1,19], can be imagined.

Diamondiyne is one such diamondyne structure in which sp^3-hybridized carbons are connected by four sp-hybridized carbons, thus forming two triple bonds, commonly known as a -diyne group (Fig. 1a). The linear -diyne group conserves the diamond topology but expands the crystal structure, making it more porous (Fig. 1a).

There are two challenges in the synthesis of diamondiyne. Firstly, along with the synthesis of the silicon homolog of diamondiyne in 2021, it was suggested that the carbon version was unreachable because of low stability of tetraethynylmethane in its unprotected form[20]. Secondly, in the research field of covalent organic frameworks, covalent crystals are built from monomers in a predesigned fashion[21-23]. Typically, this is done using reversible bonds, as a self-correcting mechanism then exist to facilitate the thermodynamically most stable state, i.e., the crystalline state, to be reached. However, carbon-carbon bonds are typically non-reversible, self-correction is therefore not a possible route for reaching the thermodynamically most stable state. We have focused on synthesizing 3D crystalline materials based on non-reversible bonds by applying a strict control of the kinetics of the used reaction, that is by making sure that monomers bind one-by-one to a formed crystallite[24-26].

Results and discussion

Here we report the synthesis of diamondiyne through a cascade reaction localized at a liquid-liquid interface (Fig. 1b). In the liquid-liquid solvent system, tetra(triethylsilylethynyl)methane and CuF_2 were selectively distributed in separate phases, and CuF_2 serves two purposes: Firstly, F^- works as a deprotection reagent for silyl groups, producing tetraethynylmethane, which has exposed terminal alkyne groups. Secondly, Cu^{2+} catalyzes the coupling between two terminal alkynes. By such a cascade reaction, a gradual release and instant consumption of the active

tetraethynylmethane is achieved, mitigating the low stability of the compound. Furthermore, the deprotection and coupling reactions are confined to the interface because it is where tetra(triethylsilylethynyl)methane and CuF_2 interact.

As crystallites start to cover the interface, these grow in the direction normal to the interface homogenously. We have previously shown that under such circumstances, the growth of covalent crystals follows first order kinetics with respect to the monomer used.[24-27] In contrast, the unwanted homocoupling reaction between two tetraethynylmethane in the bulk is expected to follow second order kinetics. To promote the molecule-by-molecule addition of tetraethynylmethane to the diamondiyne film at the interface we therefore keep the concentration of tetra(triethylsilylethynyl)methane relatively low. This low concentration regime is facilitated by the gradual deprotection of tetra(triethylsilylethynyl)methane by F^-.

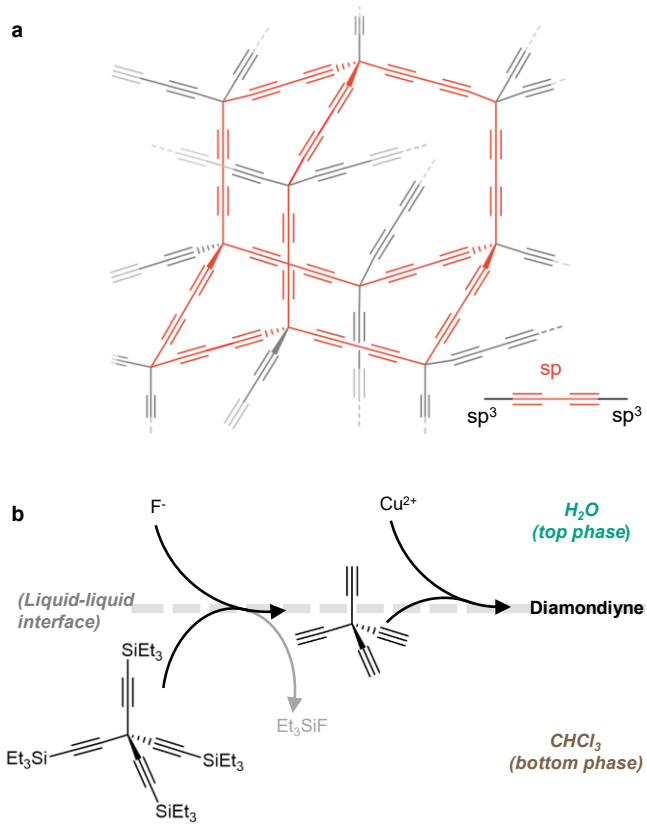

Fig. 1| The structure and synthesis of diamondiyne. a) Three-dimensional network of diamond topology in which the chemical structure contains sp- and sp^3-hybridized carbons in an 8 to 1 ratio, and forms a face-centered cubic crystal structure. b) Schematic illustration of the cascade reaction at the liquid-liquid interface, with a chloroform phase below and an aqueous phase above.

The liquid-liquid interfacial synthesis approach produces diamondiyne in the form of thin films that can reach up to 2.5 cm in diameter (Fig. 2 a-c and Supplementary Fig. 1). The film appears homogeneous under an optical microscope, albeit exhibiting some wrinkles that resulted from the transfer operation to a silicon wafer prior to analysis (Fig. 2a). An atomic force microscopy (AFM) scan over the film unveils a smooth surface without any observable pinholes or cracks (Fig. 2b). This illustrates a good uniformity and continuity, also corroborated by scanning electronic microscope (SEM; Fig 2c). The extracted sectional profile from the AFM height image along the edge of the film shows a thickness of 16 nm. Films with different thicknesses, from several nanometers to tens of nanometers, can be synthesized by controlling the reaction time (Extended Data Fig. 1). The material thickness follows a linear correlation with reaction time (Fig. 2d), indicating that mass transfer of catalyst and/or monomers through the film is not limiting the reaction rate. Shorter reaction times can therefore be used to generate very thin films (<5 nm) that, however, exhibit limited robustness for subsequent transfer operation (Extended Data Fig. 2 a-b). Conversely, longer reaction times can be used to generate thicker films with sufficient robustness to transfer pieces with an area of 10^4-10^5 square micrometers (Extended Data Fig. 2 c-d).

To validate that the deprotection and coupling reactions proceed as anticipated, we have studied the reactant, diamondiyne and a model compound (hexa-2,4-diyne) using Fourier transform infrared (FTIR) and Raman spectroscopy. The spectra of diamondiyne show relatively limited numbers of allowed transitions (Fig. 2e-f, red line, Supplementary Table 1). For instance, compared to the reactant tetra(triethylsilylethynyl)methane (blue line), signals from C-H stretching vibrations (2873-2956 cm^{-1}) are absent in diamondiyne, indicating no residual silyl protection

groups in the film. Furthermore, the terminal alkynes of the deprotected reactant have a characteristic C-H stretching vibration (3300 cm^{-1}; green line). The absence of this vibration in diamondiyne suggests that there are no residual intermediates remaining in the structure.

The C≡C stretching vibrational modes associated with alkynes are Raman active for the model compound hexa-2,4-diyne (2261 cm^{-1}; brown line) and the monomer tetra(triethylsilylethynyl)methane (2192 cm^{-1}; blue line)[28]. The low intensity of these vibrational modes when using FTIR are most likely due to the high symmetry of the molecules (Supplementary Fig. 2). The C≡C stretching vibration of the diyne group in diamondiyne is relatively weak but reproducibly observed in different samples (2234 cm^{-1}; Supplementary Fig. 3). The frequency is close to that of hexa-2,4-diyne and higher than for tetra(triethylsilylethynyl)methane, which is in accordance with expectations for a -diyne group connected to non-aromatic groups, further corroborating the structure of diamondiyne. It is noticed that the Raman shift is slightly higher for diamondiyne than the reported values for the amorphous and silicon variants (2094-2139 cm^{-1})[17,20]. Finally, the fingerprint region (700-1600 cm^{-1}) shows mainly broad transitions for diamondiyne, containing little chemical and structural information.

The elemental composition of the surface and interior of films were analyzed with X-ray photoelectron (XPS) and energy-dispersive X-ray (EDX) spectroscopies, respectively. XPS shows that the major elements observed on the film surface are carbon and oxygen (Supplementary Fig. 4). The existence of oxygen can be ascribed to the oxidation of terminal alkynes on the surface of diamondiyne, as reported for amorphous carbons materials[17] and the silicon substituted analogue[20]. In comparison, EDX indicates that the interior of the film (Supplementary Fig. 5) has a relatively lower amount of oxygen defects. Furthermore, only minor traces of encapsulated F^- can be found.

That metal catalysts can be encapsulated into framework materials has been shown before and is therefore plausible[29].

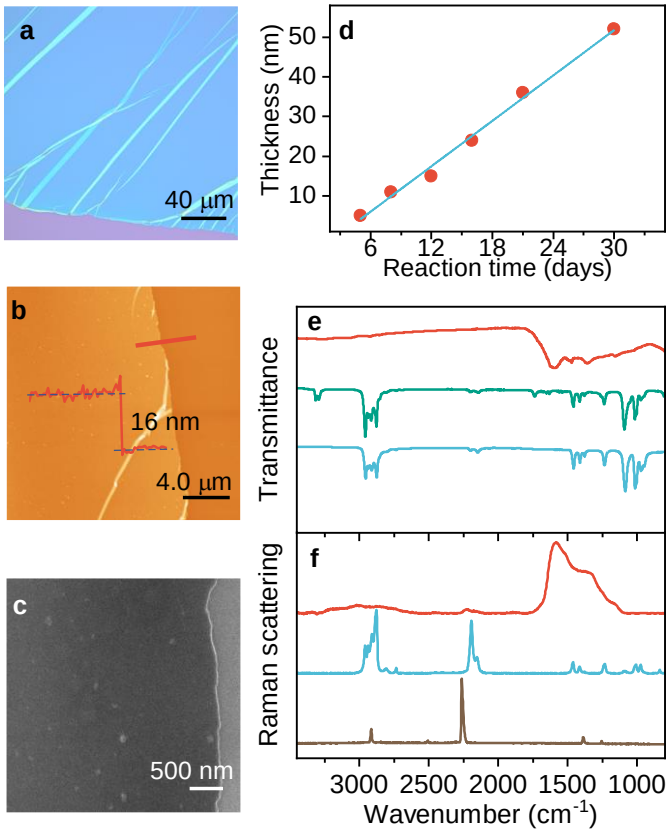

Fig. 2| Morphology and chemical characterizations of diamondiyne thin films. a) Optical microscopic image of a film on a silicon substrate. b) AFM height image of a film with a thickness of 16 nm. The inset shows the extracted sectional profile by a scan at the edge of the film. c) The SEM image of a film. d) The dependence of the film thickness as a function of reaction time. e) FTIR of diamondiyne (red), partially deprotected tetra(triethylsilylethynyl)methane (green) and tetra(triethylsilylethynyl)methane (blue). f) Raman spectra of diamondiyne (red), tetra(triethylsilylethynyl)methane (blue) and hexa-2,4-diyne (brown).

The expected crystal structure of diamondiyne forms a tetrahedral net of **dia** topology, which exhibits a face-centered cubic symmetry with a unit cell edge of 16.22 Å and space group *Fd*-3*m* (No. 227). The synthesized films show a crystalline structure with well-defined lattices under high

resolution (scanning) transmission electron microscope (HRTEM and STEM; Fig. 3a-b). Highly porous framework materials, such as COFs and MOFs are commonly found as interpenetrated structures, where several frameworks are entangled. In analogy, the sparse nature of the diamondiyne structure allows for interpenetration. HRTEM and STEM images exhibits lattice spacings consistent with the structure of both non- and interpenetrated structures of diamondiyne (Fig. 3a-b and Supplementary Tables 2-11), suggesting the existence of diamondiyne, but do not yet give any evidence for a specified phase. Note, sample-to-sample variations do exist, and several of the identified d-spacings are larger than the lowest angle reflection of the catalyst CuF_2 (Supplementary Fig. 6 and Supplementary Table 12). The monitored crystallites are thus not encapsulated catalyst but are a part of the formed carbon-based film.

The integrated differential phase contrast STEM (iDPC-STEM) image in Fig. 3b shows a 9.6 Å periodicity, however, the uneven spacing between lattice fringes suggests that interpenetrated nets are not symmetrically displaced. Furthermore, the characteristic row of reflections observed in the Fourier transform of the iDPC-STEM image (Fig. 3c), as well as in nanobeam electron diffraction (Fig. 3d-e), shows a peculiar intensity distribution. The 222 reflection is very weak while the 333, 444 and 555 reflections are stronger, which is not consistent with any diamondiyne structures having a symmetric interpenetration (Supplementary Fig. 7). However, such intensity distribution is consistent with a two-fold interpenetrated structure, where the two frameworks are displaced around 3 Å from each other (Fig. 3f, Supplementary Fig. 8, and Supplementary Tables 4&5). Furthermore, the nanobeam electron diffraction pattern obtained along the [010] direction is consistent with that predicted for the asymmetric two-fold interpenetrated diamondiyne structure (Supplementary Fig. 9). Such asymmetric displacement of interpenetrated nets has previously been observed for covalent organic frameworks[30], and its existence is probably due to the system striving to maximize van der Waals interactions between the frameworks. The asymmetric two-fold interpenetrated structure of diamondiyne can be described in the tetragonal space group $I4_1/amd$ with unit cell parameters $a=b=11.47$ Å and $c=16.22$ Å.

An iDPC-STEM image obtained along the [133] direction of the asymmetric two-fold interpenetrated structure of diamondiyne (Fig. 3g), was subjected to crystallographic image processing, where periodic information was extracted to produce a lattice averaged projected electrostatic potential map (Fig. 3h). The projected potential map is in good agreement with the

simulated iDPC-STEM image from the asymmetric two-fold interpenetrated structure (Fig. 3i, and Supplementary Figs. 10-11), providing further evidence that the structure strongly resembles a two-fold interpenetrated state with asymmetric displacement of the two carbon frameworks.

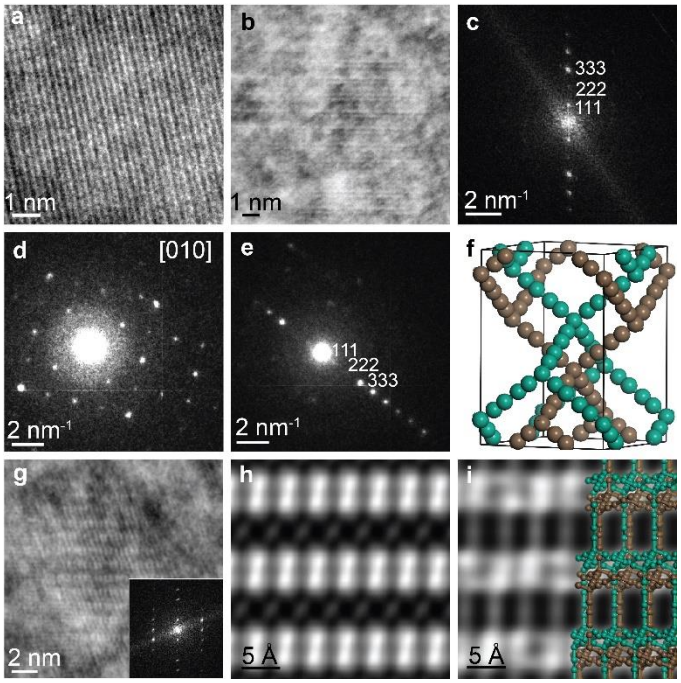

Fig. 3| Crystal structure of diamondyne. (a) High resolution TEM image of a thin film showing a periodicity of 3.4 Å, close to the 3.31 Å spacing predicted for diamondiyne. b) iDPC-STEM image showing a periodicity of 9.6 Å and an uneven spacing between fringes. c) Fourier transform of b. d) Nanobeam electron diffraction along the [010] direction and e) show the hhh family of reflections. f) Unit cell of a two-fold interpenetrated diamondiyne state, with the two nets displaced unevenly. g) iDPC-STEM image abtained along the [133] direction with the corresponding Fourier transform shown as inset. h) Lattice averaged projected electrostatic potential map of (g) with *p*2 plane group symmetry imposed. i) Simulated iDPC-STEM image along [133] with the structure of the asymmetric two-fold interpenetrated diamondyne shown overlayed.

To understand the high crystallinity apparent in diamondiyne, one needs to consider the propensity to form defects during crystal growth. Structures of diamond topology can be thought of as being composed of interconnected six-membered rings repeating in three dimensions (Fig. 1). Whereas such structures are strain free, a possible class of defects is the introduction of five membered

rings. Fig. 4 shows a computational model structure of a non-penetrated diamondiyne crystallite that contains a five membered ring defect. The zero-energy reference shown in Fig. 4 corresponds to the geometry of such a defect structure when fully relaxed. We argue that such complete defect relaxation is only possible in very small crystallites, where the strain can be distributed over the entire structure. In contrast, strain relaxation becomes less likely for crystal growth on a realistic bulk surface. We have modeled the latter by increasingly constraining sp^3-hybridized, i.e., tetrahedrally coordinated, carbon atoms to the ideal diamondiyne structure (teal atoms, Fig. 4). When mimicking a larger crystallite by constraining the structure in this way, the energy increases up to (and likely above) 18 kJ/mol per defect, which roughly equals an equilibrium constant of 10^{-3}. We emphasize that this estimate of defect relaxation is on top of the most certainly larger inherent penalty of creating a defect in the first place. We have not estimated the latter per-carbon-atom-energy as cluster models of diamondiyne and defects would require end-capping with different numbers of hydrogen. Nonetheless, we can deduce that the thermodynamics, and likely kinetic, favorability of forming the correct structure in a large crystallite clearly acts to limit defects. This in the low concentration regime, where crystallites grow by the one-by-one addition of monomers, rather than by the agglomartion of clusters. Thus, to grow covalent crystals (and framework materials in general) using non-reversible covalent bonds, the key is to use a low monomer concentration in conjunction with a framework having significant thermodynamic penelty to form errors.

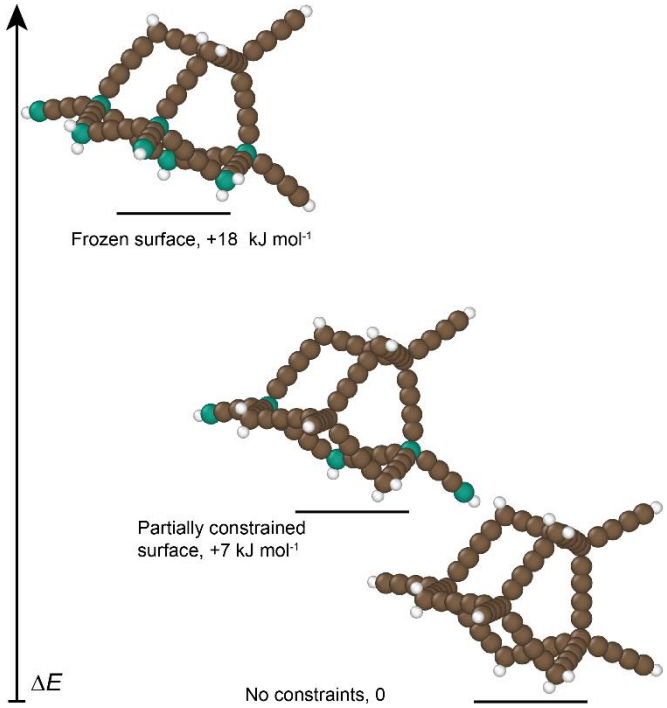

Fig. 4| Estimated cost of structural relaxation of a five membered ring defect as a function of constraint. Energies in kJ/mol are shown relative the fully relaxed defect, which is unlikely in all but the smallest crystallite seeds. Carbon atoms constrained to the correct diamondiyne structure are highlighted in green.

Conclusions

We bring the new carbon allotrope diamondiyne from the structure proposed by Feldman into reality[15]. Diamondiyne has a three-dimensional structure with diamond topology. Featuring mixed valance of hybridization, the carbon atoms are covalently connected by robust single carbon-carbon bonds and even stronger triple carbon-carbon bonds, resulting in an expanded repeating unit compared to diamond. Such irreversibly strong connections lead to the substantial synthetic challenge of inducing crystallinity throughout all three dimensions. To tackle this challenge, we have designed a cascade reaction localized to a liquid-liquid interface. By keeping the concentration of monomers low, such a reaction is kinetically directed to the crystalline state. In this manner, polycrystalline diamondiyne thin films were synthesized having continuous large

areas and controllable thickness. The porous nature of diamondiyne allows for structures within structures to form, with TEM giving evidence for a two-fold interpenetrated structure. Our work not only marks the finish for a 30-years quest, but also provides the starting point for research on a new class of carbon allotrope. The future will show if this material will be named in the same breath as diamond, graphite, graphene, fullerenes, and carbon nanotubes.

METHODS

Chemicals and Materials. All chemicals were purchased from commercial suppliers and used without further purification, including pyridine (99.8%, Merk: Sigma-Aldrich), chloroform (99.6%, VWR), CuF_2 (99.5%, Thermo scientific), hexa-2,4-diyne (98%, TCI), KF (99.9%, Merk: Sigma-Aldrich). Tetra(triethylsilylethnyl)methane was synthesized according to the literature reported procedure[17], and the received NMR spectra were in accordance with the published ones (Supplementary Figs. 12 and 13).

Diamondiyne film fabrication. Tetra(triethylsilylethynyl)methane was dissolved in chloroform to make a monomer solution with a concentration of 4 mg/mL. CuF_2 was dissolved in the mixed solvent of pyridine and milli-Q water (v:v = 1:1) to make a catalyst solution with a concentration of 25 mg/mL. 2 mL of the monomer solution was added into a vial (diameter of 2.5 cm, height of 6 cm), followed by a subsequent addition of 3 mL the catalyst solution. It was clearly observed that a stable liquid-liquid two phase system formed, with the top-phase in light blue color and a colorless bottom-phase. Then the vial was sealed and kept in a vibration free environment under ambient condition. At the liquid-liquid interface, a film was gradually formed and could be seen after about one week, with an increased thickness with an extended reaction time. When arrived at target thickness, a wash-removal procedure was carried out to get rid of the catalyst, unreacted

monomers and byproducts. For the top-phase, 5 mL milli-Q water was added and removed from the top-phase without causing disturbance at the interface. The wash-removal operation was repeated until the top-phase became completely colorless. For the bottom phase, 2 mL chloroform was slowly injected and later removed from the bottom phase three times. Finally, the diamondiyne film was obtained at the interface and could be transferred to wanted substrates.

Detection of deprotected intermediate. A tetra(triethylsilylethynyl)methane solution (5 mg/mL) in methanol was mixed with a KF solution (1 mg/mL) in methanol in a 1:1 (v/v) ratio. The mixed solution was kept under ambient condition for 30 min and then the FTIR spectrum was then measured using an ATR accessory for the detection of deprotected terminal alkyne groups.

Instrumentation. Optical microscopic images of films were captured under a Zeiss Axioscope 5 instrument. SEM microscopy was conducted using a JEOL JSM-6301F scanning electron microscope with an acceleration voltage of 15 kV. AFM characterization was performed by a NT-MDT NTEGRA scanning probe microscope instrument. The TAP-150Al-G Silicon Probes from Budget Sensor were used for AFM scans. FTIR spectra were measured by a Bruker Invenio R instrument in transmission mode. Raman spectra were recorded by a WITec alpha300 R Raman Microscope with a 488 nm laser. Nuclear magnetic resonance (NMR) spectra were recorded on a Bruker spectrometer at 600 MHz for ^{1}H and 150 MHz for ^{13}C. Chemical shifts are given in parts per million using tetramethylsilane as an internal standard. The XPS analysis was performed on an ESCALab 250Xi (Thermo Scientific) using a 200 W monochromatized Al Kα radiation. TEM was carried out using a FEI Tecnai T20 transmission electron microscope with a LaB6 electron source under the acceleration voltage of 200 kV. Scanning transmission electron microscopy (STEM) images as well as nanobeam electron diffraction patterns were obtained using a ThermoFisher Themis Z double aberration-corrected TEM. The microscope was operated at an

accelerating voltage of 300 kV. The images were acquired using a beam current of ~10 pA, a convergence angle of 16 mrad and a dwell time of 2 µs. Integrated differential phase contrast (iDPC) and annular dark field (ADF) images were obtained simultaneously. The ADF detector was set at a collection angle of 25-153 mrad. The iDPC images were formed using a segmented ADF detector at a collection angle of 6-24 mrad. A high-pass filter was applied to the iDPC images to reduce low-frequency contrast. The lattice-averaged projected potential maps were obtained by crystallographic image processing using the software CRISP[31]. Nanobeam electron diffraction patterns were obtained using a semi convergence angle of 0.9 mrad resulting in a <10 nm electron beam. The data were collected using a Medipix hybrid pixel detector (Cheetah, Amsterdam Scientific Instruments) and an exposure time of 5 ms. Simulated electron diffraction patterns were obtained based on the kinematical approximation implemented in the software CrystDiff.[32] Simulations of STEM images were made using Dr Probe.[33] A multislice simulation was conducted using an atomic model built with 3×3×3 unit cells, oriented along the [1-3-2] direction. This model was sectioned into 45 slices, each approximately 1 Å in thickness, along the probe beam direction. The residual lens aberrations, measured by the DCOR-Cs corrector installed on the ThermoFisher Themis Z, were given to the simulation. A probe beam with 16 mrad convergence semi-angle and 80 pm diameter was utilized. A four-segmented detector with a 0.38 Å per pixel sampling was simulated to generate raw datasets. The simulated iDPC images were reconstructed from simulation images using a custom Python code.

Quantum Chemical Calculations. Geometry optimization and energy evaluation were performed at the M06-2X/6-31G(d) level of theory[34] using Gaussian 16, revision B.01.[35]

Other software. Chemical structures were drawn using ChemDraw or OVITO, Graphs were plotted using Origin, lattice distances in TEM images were analysed using DigitalMicrograph, and the unit cells of the various diamondiyne isomers were constructed using Materials Studio.

REFERENCES

1 Diederich, F. & Rubin, Y. Synthetic Approaches toward Molecular and Polymeric Carbon Allotropes. *Angew. Chem., Int. Ed. Engl.* **31**, 1101-1123 (1992). https://doi.org:https://doi.org/10.1002/anie.199211013

2 Hirsch, A. The era of carbon allotropes. *Nat. Mater.* **9**, 868-871 (2010). https://doi.org:10.1038/nmat2885

3 Kaiser, K. *et al.* An sp-hybridized molecular carbon allotrope, cyclo[18]carbon. *Science* **365**, 1299-1301 (2019). https://doi.org:doi:10.1126/science.aay1914

4 Sun, L. *et al.* On-surface synthesis of aromatic cyclo[10]carbon and cyclo[14]carbon. *Nature* **623**, 972-976 (2023). https://doi.org:10.1038/s41586-023-06741-x

5 Gao, Y. *et al.* On-surface synthesis of a doubly anti-aromatic carbon allotrope. *Nature* **623**, 977-981 (2023). https://doi.org:10.1038/s41586-023-06566-8

6 Haley, M. M. On the road to carbyne. *Nat. Chem.* **2**, 912-913 (2010). https://doi.org:10.1038/nchem.884

7 Patrick, C. W. *et al.* Masked alkynes for synthesis of threaded carbon chains. *Nat. Chem.* **16**, 193-200 (2024). https://doi.org:10.1038/s41557-023-01374-z

8 Arora, A. *et al.* Monodisperse Molecular Models for the sp Carbon Allotrope Carbyne; Syntheses, Structures, and Properties of Diplatinum Polyynediyl Complexes with PtC20Pt to PtC52Pt Linkages. *ACS Cent. Sci.* **9**, 2225-2240 (2023). https://doi.org:10.1021/acscentsci.3c01090

9 Fan, Q. *et al.* Biphenylene network: A nonbenzenoid carbon allotrope. *Science* **372**, 852-856 (2021). https://doi.org:doi:10.1126/science.abg4509

10 Pan, F. *et al.* Long-range ordered porous carbons produced from C60. *Nature* **614**, 95-101 (2023). https://doi.org:10.1038/s41586-022-05532-0

11 Meirzadeh, E. *et al.* A few-layer covalent network of fullerenes. *Nature* **613**, 71-76 (2023). https://doi.org:10.1038/s41586-022-05401-w

12 Hou, L. *et al.* Synthesis of a monolayer fullerene network. *Nature* **606**, 507-510 (2022). https://doi.org:10.1038/s41586-022-04771-5

13 Li, H. *et al.* Graphynes and Graphdiynes for Energy Storage and Catalytic Utilization: Theoretical Insights into Recent Advances. *Chem. Rev.* **123**, 4795-4854 (2023). https://doi.org:10.1021/acs.chemrev.2c00729

14 Zheng, Z., Xue, Y. & Li, Y. A new carbon allotrope: graphdiyne. *Trends Chem.* **4**, 754-768 (2022). https://doi.org:https://doi.org/10.1016/j.trechm.2022.05.006

15 Feldman, K. S., Weinreb, C. K., Youngs, W. J. & Bradshaw, J. D. Preparation and Some Subsequent Transformations of Tetraethynylmethane. *J. Am. Chem. Soc.* **116**, 9019-9026 (1994). https://doi.org:10.1021/ja00099a020

16 Feldman, K. S., Kraebel, C. M. & Parvez, M. Tetraethynylmethane. *J. Am. Chem. Soc.* **115**, 3846-3847 (1993). https://doi.org:10.1021/ja00062a089
17 Zhao, Z. *et al.* A 3D Organically Synthesized Porous Carbon Material for Lithium-Ion Batteries. *Angew. Chem., Int. Ed.* **57**, 11952-11956 (2018). https://doi.org:https://doi.org/10.1002/anie.201805924
18 Hoffmann, R., Kabanov, A. A., Golov, A. A. & Proserpio, D. M. Homo Citans and Carbon Allotropes: For an Ethics of Citation. *Angew. Chem., Int. Ed.* **55**, 10962-10976 (2016). https://doi.org:https://doi.org/10.1002/anie.201600655
19 Costa, D. G., Henrique, F. J. F. S., Oliveira, F. L., Capaz, R. B. & Esteves, P. M. n-Diamondynes: Expanding the family of carbon allotropes. *Carbon* **136**, 337-344 (2018). https://doi.org:https://doi.org/10.1016/j.carbon.2018.04.073
20 Yang, Z. *et al.* Porous 3D Silicon-Diamondyne Blooms Excellent Storage and Diffusion Properties for Li, Na, and K Ions. *Adv. Energy Mater.* **11**, 2101197 (2021). https://doi.org:https://doi.org/10.1002/aenm.202101197
21 Diercks, C. S. & Yaghi, O. M. The atom, the molecule, and the covalent organic framework. *Science* **355**, eaal1585 (2017). https://doi.org:doi:10.1126/science.aal1585
22 Yang, Y. & Börjesson, K. Electroactive covalent organic frameworks: a new choice for organic electronics. *Trends Chem.* **4**, 60-75 (2022). https://doi.org:10.1016/j.trechm.2021.10.007
23 Yang, Y. *et al.* Electroactive Covalent Organic Framework Enabling Photostimulus-Responsive Devices. *J. Am. Chem. Soc.* **144**, 16093-16100 (2022). https://doi.org:10.1021/jacs.2c06333
24 Yang, Y., Schäfer, C. & Börjesson, K. Detachable all-carbon-linked 3D covalent organic framework films for semiconductor/COF heterojunctions by continuous flow synthesis. *Chem* **8**, 2217-2227 (2022). https://doi.org:https://doi.org/10.1016/j.chempr.2022.05.003
25 Yang, Y., Ratsch, M., Evans, A. M. & Börjesson, K. Layered 3D Covalent Organic Framework Films Based on Carbon–Carbon Bonds. *J. Am. Chem. Soc.* **145**, 18668-18675 (2023). https://doi.org:10.1021/jacs.3c06621
26 Yang, Y. *et al.* A Highly Conductive All-Carbon Linked 3D Covalent Organic Framework Film. *Small* **17**, 2103152 (2021). https://doi.org:https://doi.org/10.1002/smll.202103152
27 Yang, Y. *et al.* A self-standing three-dimensional covalent organic framework film. *Nat. Commun.* **14**, 220 (2023). https://doi.org:10.1038/s41467-023-35931-4
28 Bakthavatsalam, S., Dodo, K. & Sodeoka, M. A decade of alkyne-tag Raman imaging (ATRI): applications in biological systems. *RSC Chem. Biol.* **2**, 1415-1429 (2021). https://doi.org:10.1039/D1CB00116G
29 Ratsch, M. *et al.* All-Carbon-Linked Continuous Three-Dimensional Porous Aromatic Framework Films with Nanometer-Precise Controllable Thickness. *J. Am. Chem. Soc.* **142**, 6548-6553 (2020). https://doi.org:10.1021/jacs.9b10884
30 Gong, C. *et al.* Synthesis and Visualization of Entangled 3D Covalent Organic Frameworks with High-Valency Stereoscopic Molecular Nodes for Gas Separation. *Angew. Chem., Int. Ed.* **61**, e202204899 (2022). https://doi.org:https://doi.org/10.1002/anie.202204899
31 Hovmöller, S. CRISP: crystallographic image processing on a personal computer. *Ultramicroscopy* **41**, 121-135 (1992). https://doi.org:https://doi.org/10.1016/0304-3991(92)90102-P
32 CrystDiff (Zenodo, 2019).

33 Barthel, J. Dr. Probe: A software for high-resolution STEM image simulation. *Ultramicroscopy* **193**, 1-11 (2018). https://doi.org:https://doi.org/10.1016/j.ultramic.2018.06.003
34 Zhao, Y. & Truhlar, D. G. The M06 suite of density functionals for main group thermochemistry, thermochemical kinetics, noncovalent interactions, excited states, and transition elements: two new functionals and systematic testing of four M06-class functionals and 12 other functionals. *Theor. Chem. Acc.* **120**, 215-241 (2008). https://doi.org:10.1007/s00214-007-0310-x
35 Gaussian 16 Rev. B.01 (Wallingford, CT, 2016).
36 Zhang, S., Fu, Y. Q., Bui, X. L. & Du, H. J. XPS Study of diamond-like carbon-based manocomposite films. *Int. J. Nanosci.* **03**, 797-802 (2004). https://doi.org:10.1142/s0219581x04002693
37 Artemenko, A., Kozak, H., Biederman, H., Choukourov, A. & Kromka, A. Amination of NCD Films for Possible Application in Biosensing. *Plasma Processes Polym.* **12**, 336-346 (2015). https://doi.org:https://doi.org/10.1002/ppap.201400151
38 Hay, A. S. Oxidative coupling of acetylenes. II. *J. Org. Chem.* **27**, 3320-3321 (1962).

Supplementary Information is available for this paper.

Acknowledgements We acknowledge instrumental support from the Chalmers Materials Analysis Laboratory (CMAL), the MC2 Chalmers Nanofabrication Laboratory, and the Swedish Research Council and Swedish Foundation for Strategic Research for access to ARTEMI, the Swedish National Infrastructure in Advanced Electron Microscopy (2021-00171 and RIF21-0026). K.B gratefully acknowledges the financial support from the Göran Gustafsson foundation and the Knut and Alice Wallenberg Foundation (KAW 2017,0192). This research relied on computational resources provided by the National Academic Infrastructure for Supercomputing in Sweden (NAISS) at C3SE and NSC partially funded by the Swedish research council through grant agreement no. 2018-05973. T.W. acknowledge the Swedish Research Council (VR, 2019-05465). T.W. and Y.X. acknowledge the Carl Trygger Foundation for a postdoc grant (CTS 20:471).

Author contributions Y.Y. conducted the majority of the diamondiyne film experiments and analyzed the results; J.X. conducted some of the diamondiyne film experiments; Y.C. performed

TEM and Raman characterizations; Y.X. performed the STEM simulations; C.S. synthesized the starting material; M.R. did initial studies on the synthesis of the starting material; M.R. directed the research interest towards carbon allotropes and performed theoretical analysis; T.W. performed STEM and electron diffraction characterization and crystal structure analysis; K.B. conceived the idea of which allotrope that should be targeted, how it should be synthesized, and initiated and supervised the project. All the authors contributed to writing the manuscript.

Author Information The authors declare no competing financial interests. Correspondence should be addressed to K.B (karl.borjesson@gu.se).

Extended Data

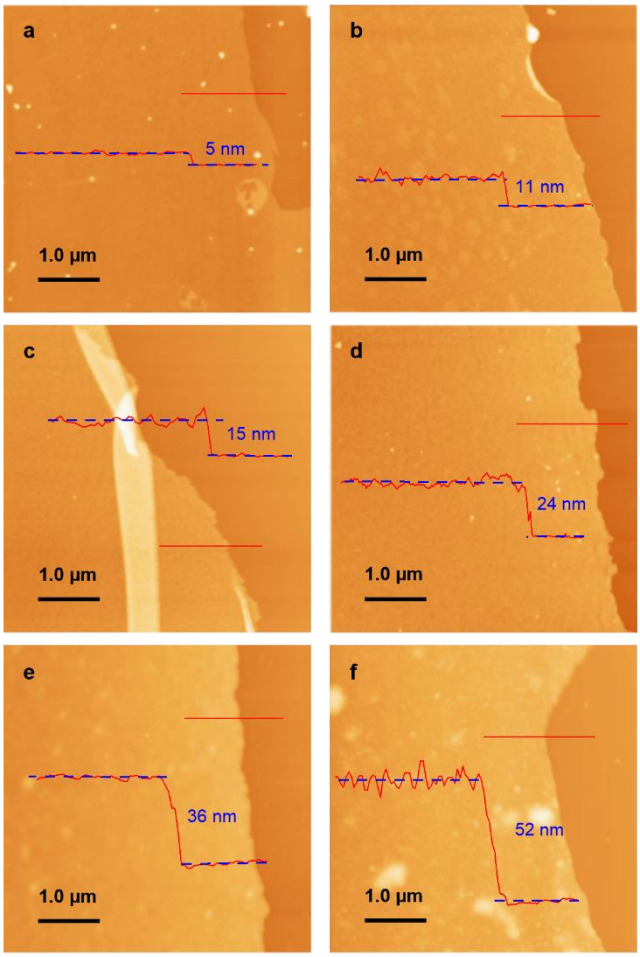

Extended Data Fig. 1| AFM height images of diamondiyne films with different thicknesses. All the films were synthesized by the same method but with different reaction time ranging from 5 days (a), 8 days (b), 12 days (c), 16 days (d), 21 days (e), to 30 days (f).

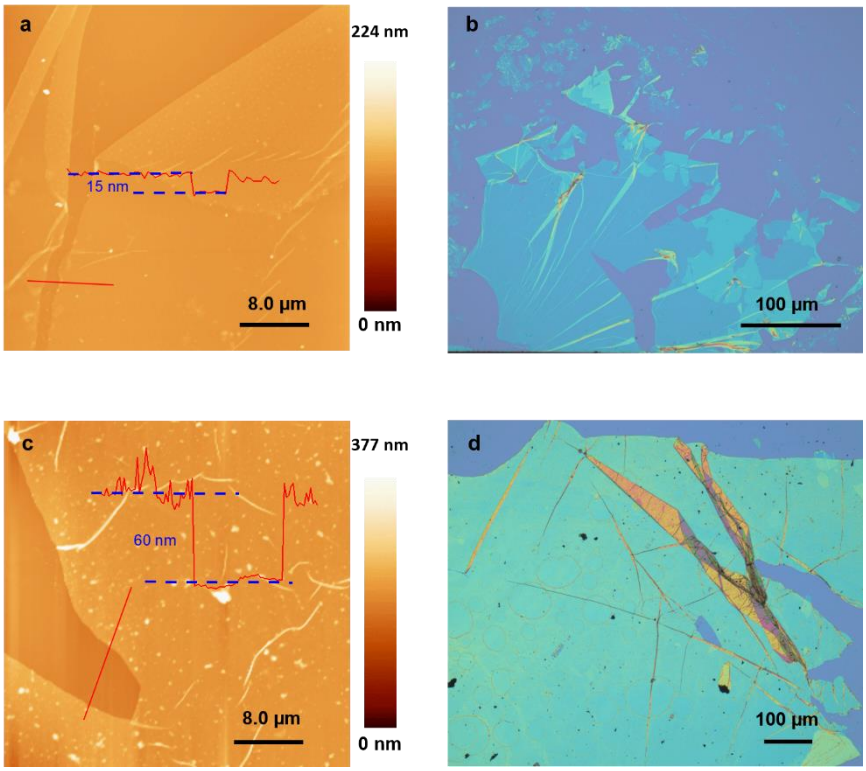

Extended Data Fig. 2| Diamondiyne films transferred to substrates with short and long reaction times. AFM heigh image (a) and optical microscopy image (b) of a diamondiyne film, made with a reaction time of 12 days, and transferred to a silicon wafer. AFM heigh image (c) and optical microscopy image (d) of a film, made with a reaction time of 30 days, and transferred to a silicon wafer.

Supplementary Information

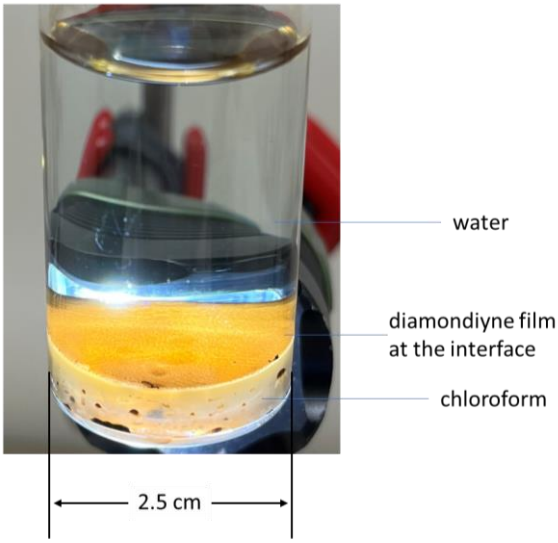

Supplementary Fig. 1| Diamondiyne film formed at the interface of a liquid-liquid interfacial system. The top phase and the bottom phases consist of milli-Q water and chloroform, respectively. The films cover the whole interface area of 9.6 cm^2. A flashlight is backlighting the liquid, giving the film a yellow color and the chloroform phase a pale opaque color.

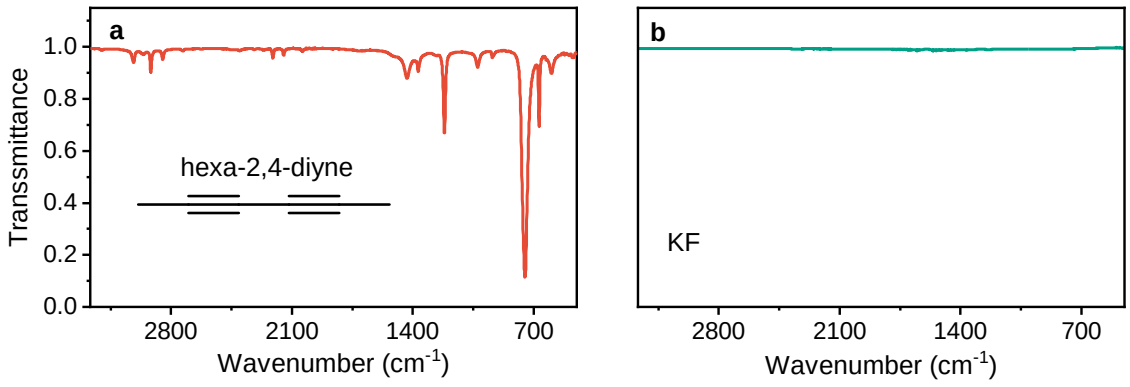

Supplementary Fig. 2| Additional FTIR spectra. (a) FTIR spectrum of hexa-2,4-diyne. (b) FTIR spectrum of KF (used as a deprotection reagent when capturing the intermediate species, i.e. the terminal alkyne) showing no signal in the observed range.

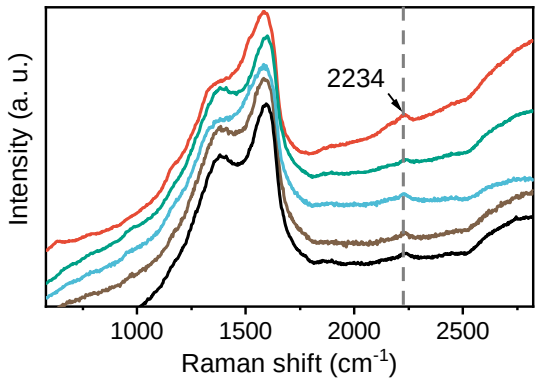

Supplementary Fig. 3| Raman spectra of diamondiyne films. Spectra were collected from film samples of 5 batches that were synthesized with the same method. All spectra show the weak peak at 2234 cm^{-1} of the -diyne group.

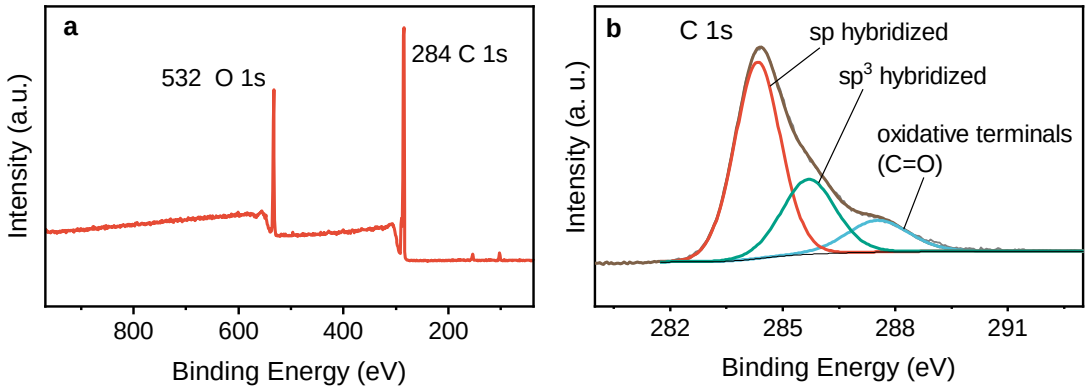

Supplementary Fig. 4| XPS of a diamondiyne film. (a) XPS survey spectrum of the diamondiyne film. (b) High-resolution XPS scan spectrum of the C 1s peak of the film. The high resolution XPS of C 1s can be deconvoluted to three peaks, at 284.4, 285.7 and 287.6 eV, corresponding to sp-C, sp^3-C and the oxidized C[20,36,37]. The ratio between sp-C and sp^3-C are 2.6:1, which is lower than the expected value of 8:1. This is due to an oxidation of terminal alkynes is consuming sp-C on the surface of the film, resulting in the observed ratio being lower than the expectation[17]. Note that it is not possible to perform the reaction under inert atmosphere as to remove the possibility for terminal alkynes to be oxidized. This is because molecular oxygen is used as an oxidation agent for Cu in the reaction mechanism to promote the reaction rate.[38]

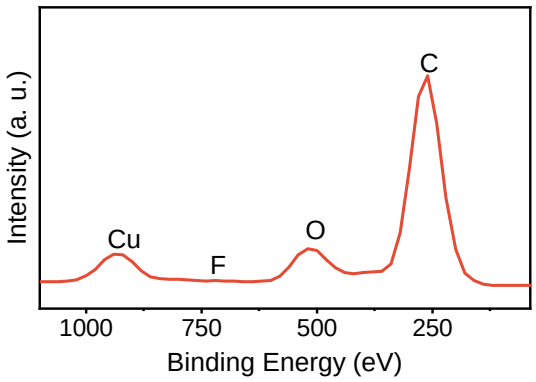

39

40 **Supplementary Fig. 5| EDX of a diamondiyne film.** EDX of a diamondiyne film that is
41 supported by a standard Cu-grid used in the TEM measurements. The expected binding energies
42 of relevant elements are indicated. Note that the large Cu signal is due to the Cu-grid used.

43

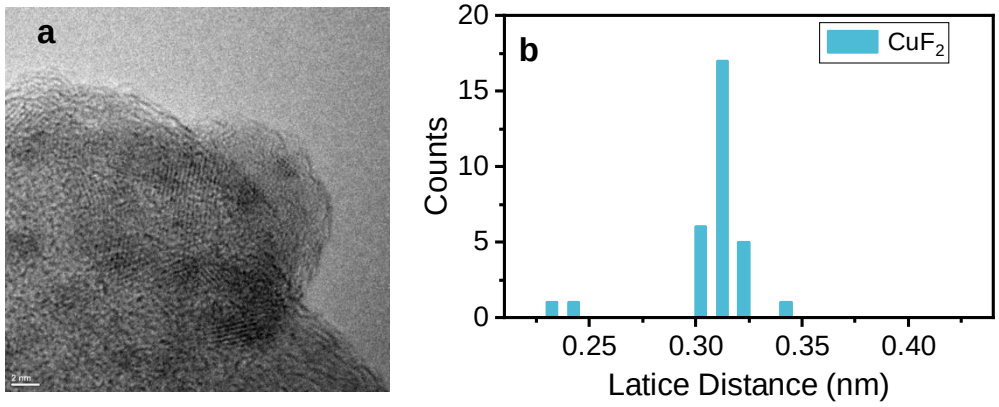

44

45 **Supplementary Fig. 6| Example of a TEM and d-spacings of CuF_2.** CuF_2 was drop cast on a
46 TEM grid. (a) An example of a TEM image of CuF_2. (b) Statistics of d-spacings taken from several
47 TEM images. The most common lattice distance corresponds to the hkl=011 reflection, which is
48 predicted to be at 3.23 Å (Supplementary Table 12).

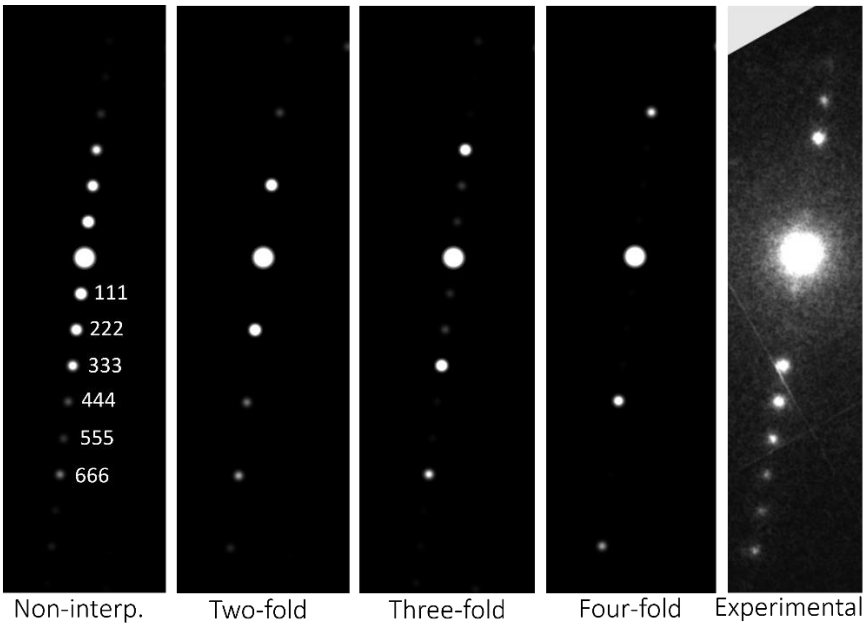

49

50 **Supplementary Fig. 7| Simulations of diffraction intensities of diamondiyne having different**

51 **interpenetration.** Simulations of electron diffraction intensities from the *hhh* systematic row for

52 diamondiyne structures of different degrees of interpenetration.

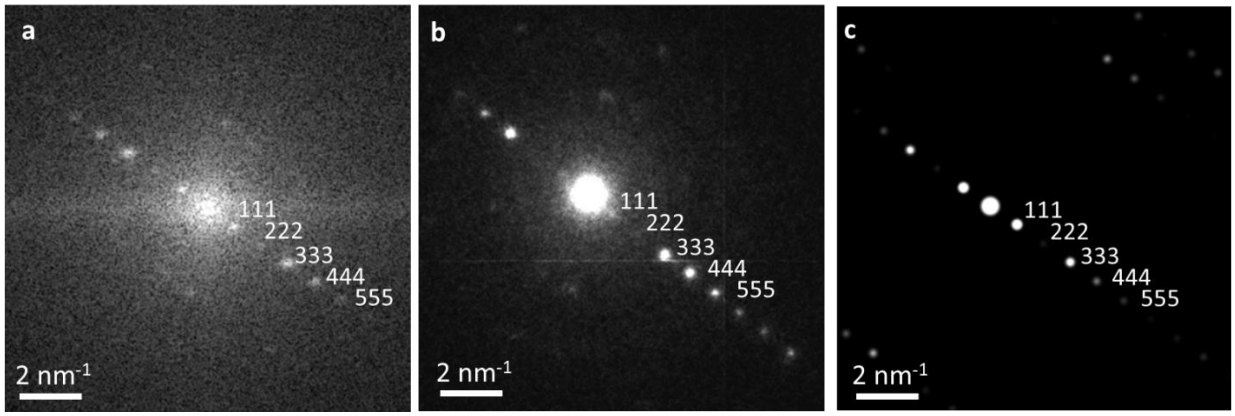

Supplementary Fig. 8| Experimental and simulated diffraction intensities of asymmetric two-fold interpenetrated diamondiyne. (a) Fourier transform of an iDPC-STEM image that show the hhh family of reflections. Note that 222 is very weak in intensity. (b) Nanobeam electron diffraction pattern from a small crystallite of diamondyne showing the hhh family of reflections. (c) Simulated electron diffraction pattern based on the 2-fold interpenetrated structure of diamondyne.

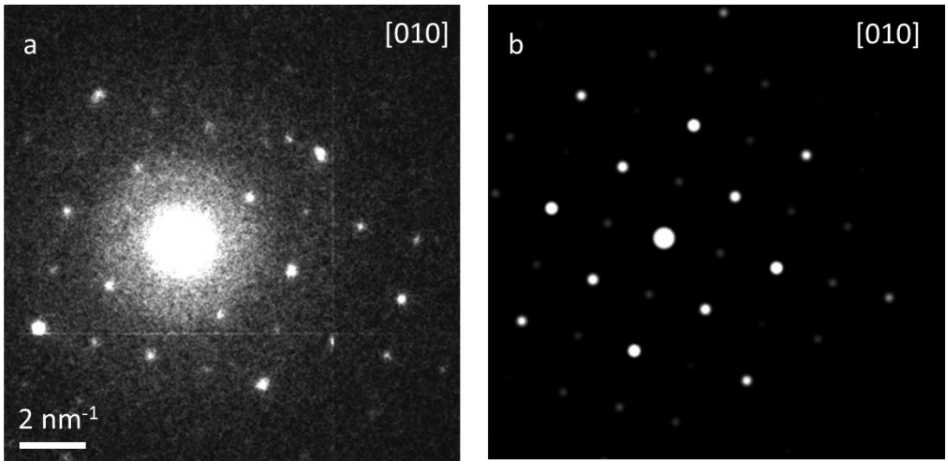

Supplementary Fig. 9| Experimental and simulated diffraction intensities of asymmetric two-fold interpenetrated diamondiyne. (a) Nanobeam electron diffraction pattern using a beam size of ~10 nm obtained along the [010] orientation of diamondiyne. (b) Simulated electron diffraction pattern along [010] using the 2-fold interpenetrated structure with asymmetric interpenetration.

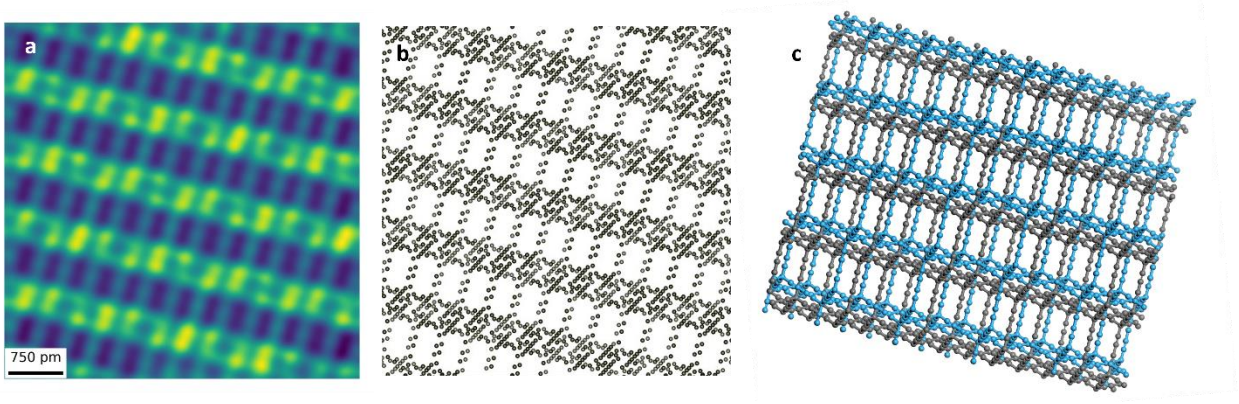

Supplementary Fig. 10| Simulating the iDPC-STEM image. (a) Simulations of an iDPC-STEM image along [133]. (b) The atomic model of the 2-fold interpenetrated diamondiyne structure used for the simulation. (c) The atomic structure of the 2-fold interpenetrated diamondyne structure with each of the two frameoworks displayed in grey and blue, respectively.

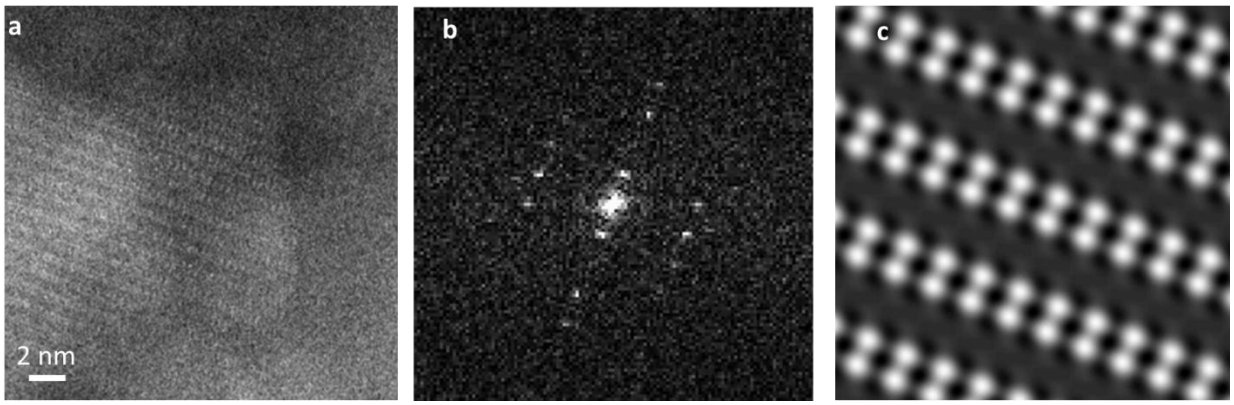

Supplementary Fig. 11| The process of producing a lattice averaged map. (a) Annular dark field-STEM (ADF-STEM) image obtained from a crystal of diamondyne along the [133] direction of the asymmetric two-fold interpenetrated structure of diamondiyne. (b) Fourier transform of the image in (a). (c) Lattice averaged map based on the periodic information from (a) with p2 plane group symmetry imposed.

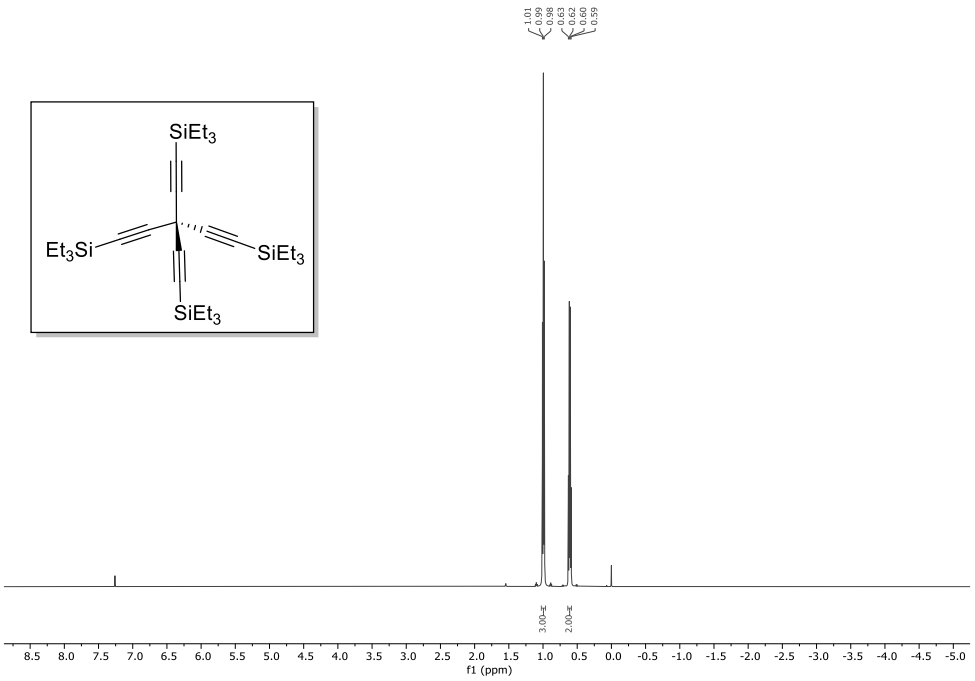

77

78 **Supplementary Fig. 12| ^{1}H NMR spectrum of tetra(triethylsilylethynyl)methane.** ^{1}H NMR

79 (600 MHz, $CDCl_3$) δ 0.99 (t, J = 7.9 Hz, 3H), 0.61 (q, J = 7.9 Hz, 2H).

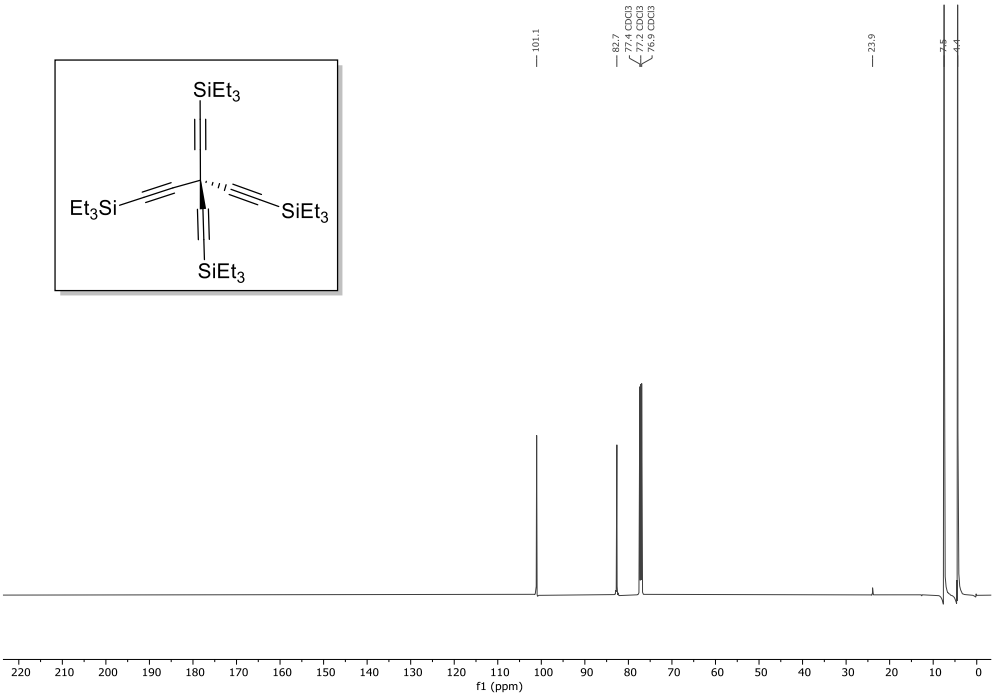

80

81 **Supplementary Fig. 13| ^{13}C NMR spectrum of tetra(triethylsilylethynyl)methane.** ^{13}C NMR

82 (151 MHz, $CDCl_3$) δ 101.1, 82.7, 77.4, 77.2, 76.9, 23.9, 7.5, 4.4.

Supplementary Tab. 1| Assignment of the major vibration signals in FTIR and Raman for the reactant, intermediate and diamondiyne.

Wavenumber (cm^{-1})	Assignment	tetra(triethylsilylethynyl)methane		Deprotected tetra(triethylsilyl-ethynyl)methane	diamondiyne	
		IR Intensity	Raman Intensity	IR Intensity	IR Intensity	Raman Intensity
3300	-C≡C-H stretching	-	-	18	-	-
2873-2956	C-H stretching	45	100	71	-	-
2234	-C≡C-C≡C- stretching	-	-	-	-	8
2192	C≡C stretching	5	84	-	-	-
2146	C≡C stretching	7	28	8	-	-
1580	-C≡C-C≡C- bending	-	-	-	100	100
1456	C-H bending	30	20	28	-	-
1349	-C-C≡C- stretching	-	-	-	86	51
1084	C-C stretching	60	8	61	-	-
720	C-H bending	100	-	100		-

Supplementary Tab. 2| Atomic coordinates for the non-interpenetrated diamondiyne crystal structure.

Space group: *Fd*-3*m*

Unit cell: a = b = c = 16.222 Å, α = β = γ = 90°

Atom	**x**	**y**	**z**
C1	0.250000	0.750000	0.750000
C2	0.195900	0.695900	0.695900
C3	0.152560	0.847440	0.847440

Supplementary Tab. 3| Predicted d-spacings for the simulated diamondiyne crystal

h	k	l	d-spacing	Amplitude
1	1	1	9.37	100.82
0	2	2	5.74	68.82
1	3	1	4.89	6.05
2	2	2	4.68	72.40
4	0	0	4.06	19.66
1	3	3	3.72	3.72
2	2	4	3.31	16.49
1	5	1	3.12	15.42
3	3	3	3.12	44.56
0	4	4	2.87	46.18
1	5	3	2.74	2.66
2	4	4	2.70	49.08
0	2	6	2.56	18.81
3	5	3	2.47	30.79

Supplementary Tab. 4| Atomic coordinates for the simulated diamondiyne crystal structure with unsymmetric two-fold interpenetration

Space group: $I4_1/amd$

Unit cell: a = b = 11.471 Å, c = 16.222 Å, $\alpha = \beta = \gamma = 90^{o}$

Atom	x	y	z
C1	0.00000	0.00000	0.12708
C2	0.00000	0.89180	0.18118
C3	0.00000	0.19488	0.22452
C4	0.39180	0.50000	0.57298
C5	0.69488	0.50000	0.52964

Supplementary Tab. 5| Predicted d-spacings for the simulated diamondiyne crystal with unsymmetric two-fold interpenetration

h	k	l	d-spacing	Amplitude
0	1	1	9.37	70.36
2	0	0	5.74	68.82
1	1	2	5.74	1.80
1	0	3	4.89	4.44
2	1	1	4.89	4.22
2	0	2	4.68	1.89
2	2	0	4.06	19.66
3	0	1	3.72	40.38
2	1	3	3.72	42.49
0	2	4	3.31	16.47
1	3	2	3.31	0.43
3	0	3	3.12	32.76
1	0	5	3.12	10.17
2	3	1	3.12	10.76
2	2	4	2.87	46.11
4	0	0	2.87	46.18
1	4	1	2.74	1.86
1	2	5	2.74	1.76
2	3	3	2.74	1.95
3	1	4	2.70	49.01
4	0	2	2.70	1.28
2	4	0	2.56	18.81
1	1	6	2.56	1.47
3	3	2	2.56	0.49
3	0	5	2.47	20.30
4	1	3	2.47	22.61

Supplementary Tab. 6| Atomic coordinates for the simulated diamondiyne crystal structure with symmetric two-fold interpenetration

Space group: *Pn*-3*m*

Unit cell: a = b = c = 8.111 Å, $\alpha = \beta = \gamma = 90^{o}$

Atom	x	y	z
C1	0.50000	0.50000	0.50000
C2	0.39177	0.39177	0.39177
C3	0.30509	0.69491	0.69491

Supplementary Tab. 7| Predicted d-spacings for the simulated diamondiyne crystal structure with symmetric two-fold interpenetration

h	k	l	d-spacing	Amplitude
1	1	0	5.74	17.20
1	1	1	4.68	18.11
2	0	0	4.06	4.93
2	1	1	3.31	4.12
2	0	2	2.87	11.55
1	2	2	2.70	12.27
1	3	0	2.57	4.70
1	1	3	2.45	1.11
2	2	2	2.34	2.17
1	2	3	2.17	4.09

Supplementary Tab. 8| Atomic coordinates for the simulated diamondiyne crystal structure with three-fold interpenetration

Space group: $I4_1/amd$

Unit cell: a = b = 11.471 Å, c = 5.407, $\alpha = \beta = \gamma = 90^{o}$

	x	y	z
C1	0.50000	0.00000	0.75
C2	0.50000	0.10820	0.91230
C3	0.50000	0.80512	0.04232

Supplementary Tab. 9| Predicted d-spacings for the simulated diamondiyne crystal structure with three-fold interpenetration

h	k	l	d-spacing	Amplitude
2	0	0	5.74	34.41
1	0	1	4.89	3.03
2	2	0	4.06	9.83
2	1	1	3.72	28.93
3	0	1	3.12	22.28
4	0	0	2.87	23.09
3	2	1	2.74	1.33
4	2	0	2.56	9.41
4	1	1	2.47	15.40

Supplementary Tab. 10| Atomic coordinates for the simulated diamondiyne crystal structure with four-fold interpenetration

Space group: *P4/nbm*

Unit cell: a = b = 8.111, c = 4.056 Å, $\alpha = \beta = \gamma = 90^{o}$

	x	y	z
C1	0.00000	0.50000	0.00000
C2	0.89180	0.39180	0.78360
C3	0.19488	0.69488	0.61024

Supplementary Tab. 11| Predicted d-spacings for the simulated diamondiyne crystal structure with four-fold interpenetration

h	k	l	d-spacing	Amplitude
1	1	0	5.74	17.21
2	0	0	4.06	4.92
1	1	1	3.31	4.12
2	2	0	2.87	11.54
1	2	1	2.70	12.27
1	3	0	2.57	4.70
2	2	1	2.34	2.16
1	3	1	2.17	4.10

Supplementary Tab. 12| Predicted d-spacings for CuF_2

h	k	l	d-spacing
0	1	1	3.23
1	0	1	2.82
1	1	0	2.66
1	0	-1	2.53
1	1	1	2.4
0	0	2	2.29
0	2	0	2.81
1	1	-1	2.21
0	1	2	2.05
0	2	1	2.04